A Virtual-Flux Decoupling Hysteresis Current Controller for Mains Connected Inverter Systems

L. A. Serpa, S. D. Round and J. W. Kolar

Swiss Federal Institute of Technology (ETH) Zurich
Power Electronics Systems Laboratory
ETH-Zentrum / ETL H16, CH-8092 Zurich, Switzerland
e-mail: {serpa, round, kolar}@lem.ee.ethz.ch

Abstract - This paper proposes a new simple method of three-phase, sensorless mains voltage, power control with near constant switching frequency based on a decoupling hysteresis current controller and the virtual-flux concept. The virtual-flux method is used to extract the mains voltage from the switching state, dc voltage and line currents. From the desired real and reactive powers the three-phase currents are generated using a decoupling hysteresis current controller. The decoupling hysteresis controller avoids the switching interaction between the phases, and when a variable hysteresis band is employed a near constant switching frequency is achieved. The method is also extended for high power inverter applications that include an LCL output filter, where some undesirable characteristics, such as filter resonance, have to be compensated. Theoretical analysis is presented and the performance of the proposed method is experimental verified.

I. INTRODUCTION

Three-phase voltage source inverters are employed in many mains connected applications, including UPS and distributed generating systems. In these applications appropriate regulation of the power flow is required and this can be achieved by either direct current control or a power regulation method. The direct current control method includes voltage oriented control and current hysteresis control (CHC) and for power regulation, Direct Power Control (DPC) is usually employed.

For mains connected applications the ideal requirements of the inverter includes a fast dynamic response, near constant switching frequency and a reduced number of sensors. However, all of these characteristics are not found in any of the standard control methods. For instance the voltage oriented control method guarantees a high static performance via an internal current control loop but suffers from a low dynamic performance [1]. For the CHC the current instantaneously follows any change in the reference and the implementation is relatively simple, however the switching frequency variable. The DPC method controls the active and reactive power by using two hysteresis controllers to select the switching state from a switching table [2]. The DPC method has a fast and robust response to transients as it behaves like the current hysteresis controllers, however it also has a similar drawback of a variable switching frequency. A constant switching frequency DPC can be achieved by substituting the modulation strategy from a switching table method to space-vector modulation [3]. Nevertheless, the dynamic response becomes equivalent to voltage orientated control.

For three-phase, three-wire inverters (Fig. 1) using CHC, coupling between phase currents exists since each phase current does not only depend on the corresponding applied voltage but also on the current in the other two phases [4][5]. The decoupling hysteresis control (DHC) [6][7] has been proposed for three-level rectifiers to minimize the interference between phases while maintaining all the advantages of the CHC. Reducing this phase current interaction results in the switching frequency becoming more uniform and allows for a near constant switching frequency if a variable hysteresis band is implemented.

One of the most important aspects in mains connected inverters to guarantee the correct operation of the system is the accurate and fast estimation of the active and reactive power. Normally these are calculated based on the measured mains voltage and current. However, in order to reduce the number of sensors, which gives reliability and economical advantages, a virtual-flux (VF) estimation technique is proposed [8] to replace the ac-line voltage sensors.

For high power applications a third order output filter that can achieve reduced levels of harmonics distortion at lower switching frequencies and with less total inductance is usually employed. However, systems incorporating LCL filter requires extra control effort in order to compensate some undesirable characteristics such as the filter resonance.

This paper proposes a sensorless mains voltage, direct active and reactive power controller operating with a near constant switching frequency. The basic control scheme uses the decoupling hysteresis controller combined with virtual-flux and power estimation methods so that the advantages of both concepts (DHC and VF-DPC), such as fast dynamic response and relatively simple implementation, are maintained. In Section II the basic concept of virtual-flux estimation is discussed and the calculation of phase currents references based on power quantities is given. In order to reduce the interference between phases the CHC is replaced by a DHC in Section III and a near constant switching frequency is achieved by adding a variable hysteresis band. Section IV experimentally illustrates the performance of the proposed system. Section V extends the virtual-flux decoupling hysteresis control (VF-DHC) for high power applications, where a third order LCL filter is necessary. Finally, Section VI verifies experimentally the extended method.

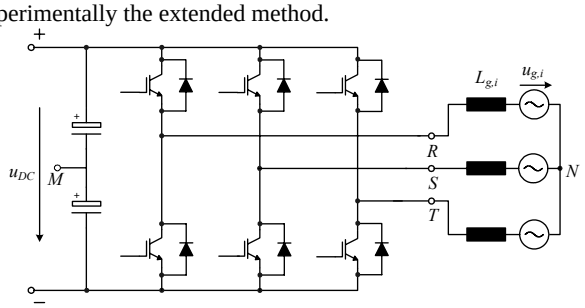

Fig. 1 - Three-Phase Two-Level Voltage Source Inverter.

II. VIRTUAL-FLUX HYSTERESIS CONTROL

Recently the Virtual-Flux (VF) strategy was proposed [8] to be added to the conventional DPC in order to replace the ac-line voltage sensor. The VF strategy assumes that the line voltage and the ac-side inductors are quantities related to a virtual ac motor. Making an analogy with ac motors, R_g and L_g (Fig. 2) represent respectively the stator resistance and the stator leakage inductance and the line voltage u_g, represents the machine's electro-motive force.

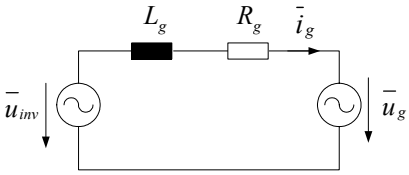

Fig. 2 -Equivalent Circuit of a mains connected Three-Phase VSI with L filter.

The mains flux calculation is based on flux definition (1) and the voltage loop equation (2).

$$\bar{\psi}_g = \int \bar{u}_g \cdot dt \tag{1}$$

$$\bar{u}_g = \bar{u}_{inv} - R_g \cdot \bar{i}_g - L_g \cdot \frac{d\bar{i}_g}{dt} \tag{2}$$

Neglecting the series resistance of the line inductor, the line virtual flux can be calculated based on the measured line current $\bar{i}_g$ and the inverter voltage $\bar{u}_{inv}$

$$\bar{\psi}_g = \int \bar{u}_{inv} \cdot dt - L_g \cdot \bar{i}_g \tag{3}$$

where the inverter output voltage in the stationary coordinates system can be calculated based on the DC link voltage and the converter switching states.

The calculated grid virtual-flux can be used to estimate the active and reactive power as follows

$$p = \frac{3}{2}\omega \cdot (\psi_{g,\alpha} \cdot i_{g,\beta} - \psi_{g,\beta} \cdot i_{g,\alpha}) \tag{4}$$

$$q = \frac{3}{2}\omega \cdot (\psi_{g,\alpha} \cdot i_{g,\alpha} + \psi_{g,\beta} \cdot i_{g,\beta}) \tag{5}$$

The CHC compares a reference current to the actual current in order to control the switching, therefore, in the proposed controller the reference currents must be first calculated from the power references and the mains virtual-flux using

$$i_{\alpha,ref} = \frac{2}{3}\frac{\psi_{g,\alpha} \cdot q_{ref} - \psi_{g,\beta} \cdot p_{ref}}{\omega \cdot \left(\psi_{g,\alpha}^2 + \psi_{g,\beta}^2\right)} \tag{6}$$

$$i_{\beta,ref} = \frac{2}{3}\frac{\psi_{g,\alpha} \cdot p_{ref} + \psi_{g,\beta} \cdot q_{ref}}{\omega \cdot \left(\psi_{g,\alpha}^2 + \psi_{g,\beta}^2\right)} \tag{7}$$

The phase quantities are then obtained by a stationary coordinates transformation and controlled by a current hysteresis controller. The combined virtual-flux current hysteresis control (VF-CHC) system is shown in Fig. 3

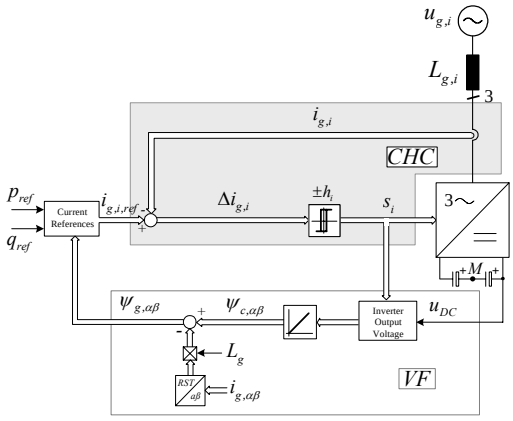

Fig. 3 - Virtual-Flux Current Hysteresis Control (VF-CHC) structure.

The strategy maintains the main characteristics of the CHC and VF-DPC, such as the fast dynamic and relatively simple implementation. On the other hand, it is also affected by the drawbacks of the interaction between phases (Fig. 4(a)) and a variable switching frequency as can be seen in the frequency spectrum and switching frequency behavior in Fig. 4(b) and Fig. 4(c).

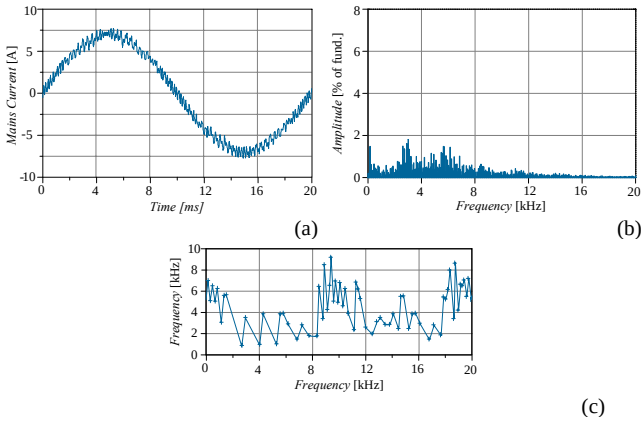

Fig. 4 - Simulated performance of VF-CHC with average switching frequency of 4kHz. The resulting mains current (a), frequency spectrum (b) and switching frequency behavior during one fundamental cycle (c).

These disadvantages can be avoided by replacing the CHC by the DHC, which decouples the phases and avoid the interaction of the switching allowing for a near constant switching frequency.

III. DECOUPLING HYSTERESIS CONTROLLER

The decoupling hysteresis controller (DHC) [6], as shown by shaded DHC area in Fig. 5, has the same basic outer structure as the standard CHC where the phase current is subtracted from a current reference and the hysteresis controller generates a switching signal from the current error. The DHC has an additional control loop that generates the current control signal, i_0. By summing the measured line current, $i_{g,i}$ with i_0, a virtual current $i'_{g,i}$ is formed. With the correct formation of i_0 the switching of the hysteresis controller can occur without any interaction between each of the phase controllers. The phase interaction is caused because the DC bus mid-point to neutral voltage is not constant, as it is dependent on each of the inverter output voltages.

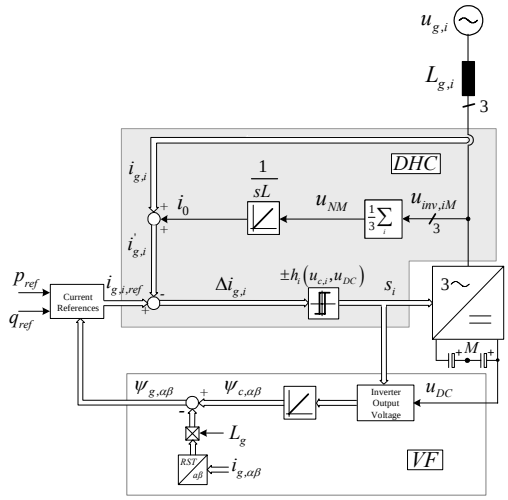

Fig. 5 - Virtual-Flux Decoupling Hysteresis Control (VF-DHC) structure.

The phase current is defined by the voltage across the output filter inductor, which is represented in Fig. 6 by the difference between the converter output voltage and the grid voltage referred to the neutral point

$$L_g \frac{di_{g,i}}{dt} = u_{L_g,i} = u_{inv,i} - u_{g,i} \qquad (i = R,S,T) \tag{8}$$

If the mains star point, *N*, and the DC mid-point, *M* are not connected (Fig. 6 (a)), then the inverter output voltage is given by

$$u_{inv,i} = u_{inv,iM} + u_{MN} \tag{9}$$

where $u_{inv,iM}$ are the inverter ac voltages referred to *M*, and u_{MN} is the zero sequence voltage occurring between the mains star point and DC mid-point.

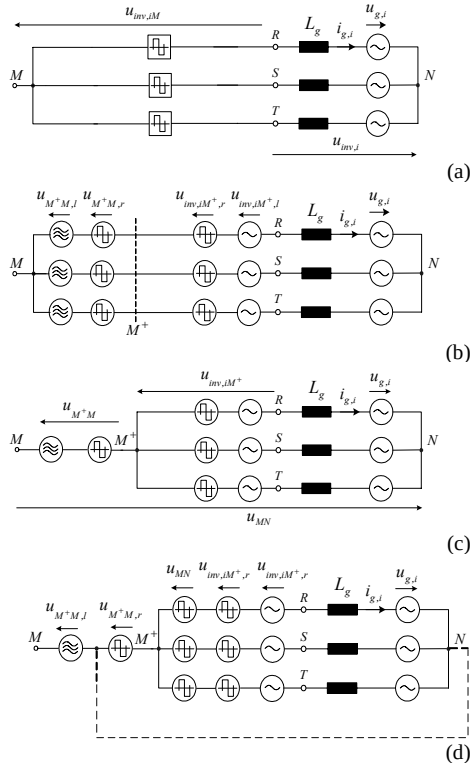

Fig. 6 - Equivalent circuits of DHC implementation (a) *M* and *N* are not connected (b) inverter output voltage divided in current forming component and zero sequence voltage (c) simplified model with the virtual potential M^+ (d) virtual connection between M^+N allowing for the high frequency decoupling between phases.

The inverter output voltage ($u_{inv,iM}$) shown in Fig. 6(a) can be split into two parts, as presented in Fig. 6(b). The first part consists of a low frequency ($u_{inv,iM^+,l}$) and a ripple ($u_{inv,iM^+,r}$) voltage of the current shaping component and the second represents the low frequency ($u_{M^+M,l}$) and ripple ($u_{M^+M,r}$) component of the zero sequence voltage.

Given that the zero sequence voltages are connected at the same potential (M^+), the equivalent circuit can be simplified to that shown in Fig. 6(c). From that, the equation which describes the inverter output voltage referred to the mid-point can be derived as follows

$$u_{inv,iM} = u_{inv,iM^+} + u_{M^+M} \tag{10}$$

or

$$u_{inv,iM} = L_g \frac{di_{g,i}}{dt} + u_{g,i} + u_{NM} \tag{11}$$

Since symmetrical mains voltage is assumed the influence of each phase on the zero sequence voltage is derived from (10)

$$u_{M^+M} = \frac{1}{3}\left(u_{inv,RM} + u_{inv,SM} + u_{inv,TM}\right) \tag{12}$$

Considering the sum of the phase currents is zero and taking (10) and (11) into account, it follows

$$u_{M^+M} = u_{NM} = -u_{MN} \tag{13}$$

Therefore, combining the equations (8), (9), (12) and (13), the coupling between the phases is clearly seen from

$$L_g \frac{di_{g,i}}{dt} = u_{inv,iM} - u_{g,i} - \frac{1}{3}\left(u_{inv,RM} + u_{inv,SM} + u_{inv,TM}\right) \tag{14}$$

The current is not only dependent on the respective inverter output voltage but is also influenced by the zero sequence voltage, represented in the equivalent circuit (Fig. 6(b)) as a high frequency switching voltage component, $u_{M^+M,r}$.

In the case where *M*, the mid-point of the DC capacitors, is directly connected to the mains neutral *N*, ($u_{MN} = 0$) and/or $u_{inv,i} = u_{inv,iM}$, there is no mechanism for any interaction between the phases. This is because the current, $i_{g,i}$, that flows in each phase is only dependent on the total voltage measured to the mid-point, $u_{inv,iM}$ as shown in (8) and (9). The fundamental current is produced by the voltage difference of the mains voltage, $u_{g,i}$, and the fundamental voltage at the output of the inverter, $u_{inv,iM,l}$. The current ripple is created from the high frequency switching voltage at the output of the inverter $u_{inv,iM,r}$.

In order to eliminate the high frequency interaction between phases for the case when the mid-point *M* and the mains neutral *N* are not connected, the ripple component of u_{M^+M} has to be cancelled and this is achieved by adding the negative of u_{M^+M}, which equals u_{MN} as proved in (13), into each of the phases as shown in Fig. 6(d). To enable the inverter to generate this extra voltage, an additional current term, i_0, is added into the current controller ($i'_{g,i} = i_{g,i} + i_0$, cf. Fig. 5). The current signal, i_0, is generated by integrating either the calculated voltage u_{M^+M} given by (12) or the measured zero sequence voltage u_{MN} as given by

$$i_0 = \frac{1}{L_g}\int u_{MN}\, dt\ . \tag{15}$$

The addition of the decoupling controller now effectively makes the point M^+ look like, from a switching frequency point of view, that it is connected to the mains neutral point (shown by dashed line in Fig. 6(d)) since $u_{M^+M,r}+u_{MN} = 0$. Thus, the high frequency switching in each phase does not have any interaction with the other two phases.

Although DHC makes the switching frequency more uniform than a CHC [7], it is desirable to have the inverter operating with a constant switching frequency as this makes the design of the output filter task simpler. The harmonic performance can be substantially improved by varying the hysteresis band over each fundamental cycle, since the switching frequency is dependent on the voltage difference across the inductor, the inductor value and the hysteresis band level.

In order to derive a relatively simple expression for the required hysteresis band it is assumed that during one switching period that the fundamental voltage is constant. The switching of the inverter either impresses a $+½u_{DC}$ (upper switch on) or a $-½u_{DC}$ (lower switch on) voltage at the inverter's ac side terminals. By combining the switching time equations and rearranging, the hysteresis band, h, required to produce a constant frequency is expressed as

$$h_i = \frac{\left(\frac{u_{DC}}{2}\right)^2 - u_{inv,i}^2}{2 \cdot L_g \cdot f_s \cdot u_{DC}} \tag{16}$$

For a sinusoidal output inverter voltage, $u_{inv,i}$, the shape of the hysteresis band for one mains period is shown in Fig. 7. The magnitude has been normalized by dividing by the peak value of the reference current.

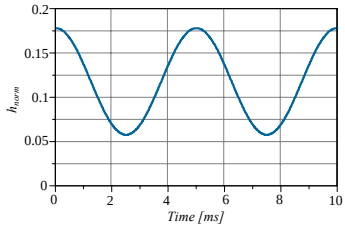

Fig. 7 - Normalized hysteresis band shape for one mains period.

The fundamental component of the inverter voltage $u_{inv,i}$ used in Eq. (16) is easily calculated from the output inverter flux ($\overline{\psi}_{inv} = \int \overline{u}_{inv} \cdot dt$) as follows

$$\begin{aligned} u_{inv,\alpha} &= -k \cdot \psi_{inv,\beta} \\ u_{inv,\beta} &= k \cdot \psi_{inv,\alpha} \end{aligned} \tag{17}$$

where k is the gain to compensate for the integrator attenuation at fundamental frequency (-50db at 50Hz).

The advantages of the VF-DHC when compared with the conventional hysteresis can be observed in the Fig. 8. Adding the zero sequence current i_0 to the actual current reduces the interference between phases (Fig. 8(a)) and allows for a near constant switching frequency in one cycle period (Fig. 8(c)) due to the modulated hysteresis band. The switching becomes more centred around 4kHz (Fig. 8(b)) rather than the wide frequency range for VF-CHC.

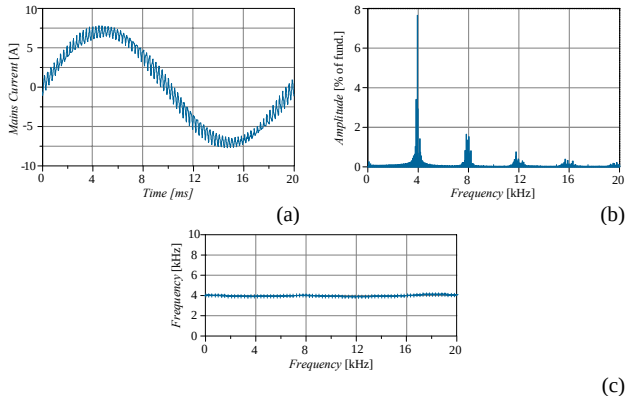

Fig. 8 - Simulated performance of the proposed VF-DHC with switching frequency of 4kHz. The resulting mains current (a), frequency spectrum (b) and switching frequency behavior during one fundamental cycle.

IV. EXPERIMENTAL VERIFICATION

In order to verify experimentally the proposed VF-DHC, it is implemented in a fully digital controller using an Analog Devices ADSP21991 16-bit 160MHz DSP interfaced to a 6kW 3-phase inverter. The output inductance of 10mH links the inverter and the controlled 400V 3-phase AC power source. The 750V DC power is provided by a 10kW, controlled DC power supply. Two phase currents and the DC voltage are sampled at 200kHz using the DSP's internal 14-bit ADC. During the ADC conversion time of 725 ns, the algorithm calculates the midpoint to neutral voltage using derived phase to midpoint voltages that are based on the switch state and previous sample instantaneous DC input voltage. The midpoint to neutral voltage is integrated and summed to the current reference. The current controller is implemented digitally using the measured phase current and references current signals. All 6 inverter switches are updated simultaneously at the end of the calculations. The calculation of the reference current and variable hysteresis band are updated at a rate of 30 kHz.

The static behaviour of proposed VF-DHC is showed in Fig. 9. From that it can be seen that the grid virtual-fluxes are successfully estimated, since the α component of the virtual flux is 90° lagging the grid voltage (phase R). The phase current is in phase with the actual supply voltage since the reactive power is controlled to be zero.

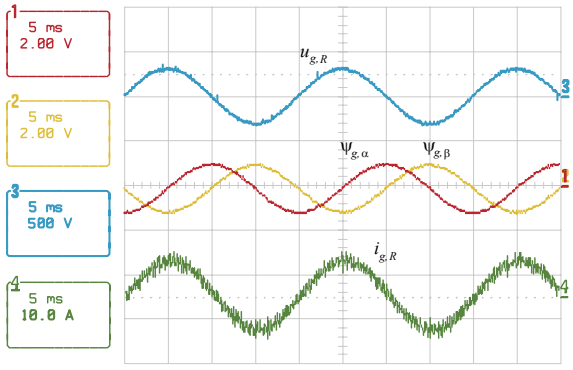

Fig. 9 – Experimental steady-state result of the mains phase voltage $u_{g.R}$, virtual-flux $\psi_{g.\alpha\beta}$ and phase-current of proposed VF-DHC.

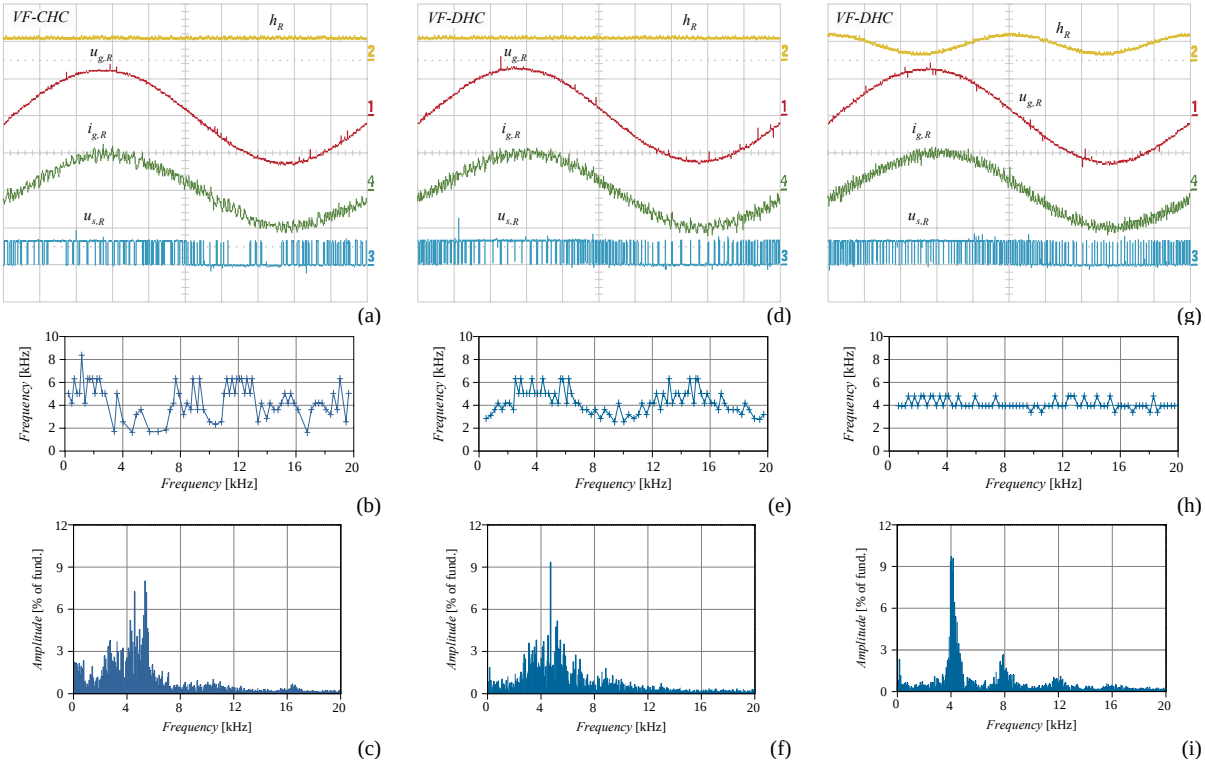

Fig. 10 – Grid voltage $u_{g.R}$, grid current $i_{g.R}$, hysteresis band h and gate signals $u_{s.R}$ of (a) VF-CHC (b) VF-DHC (c) VF-DHC with modulated hysteresis band ($u_{g.R}$ trace is 200V/div, $i_{g.R}$ is 10A/div, $u_{s.R}$ is 20V/div, time base is 2ms/div). Switching frequency behaviour during one fundamental cycle and frequency spectrum of the grid current (b)-(c) VF-CHC (e)-(f) VF-DHC (h)-(i) VF-DHC with modulated hysteresis band.

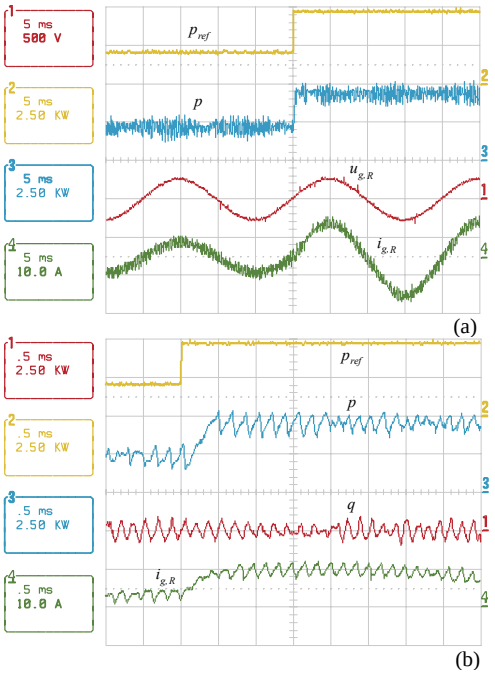

Fig. 11 – Experimental results of step response for the VF-DHC with modulated hysteresis band (a) from 40 to 80% of active power (b) detailed positive step.

The VF-DHC performance is better observed comparing the gate signals, switching frequency behaviour and the current spectrum of the proposed method with the VF-CHC and VF-DHC with constant hysteresis band. For VF-CHC (Fig. 10(a)) it can be seen for the *R* phase switching signal that there are periods where no switching occurs due to the interaction of the phases. The variable switching frequency is observed through the measured instantaneous switching frequency behaviour over one cycle period (Fig. 10 (b)) and the current spectrum (Fig. 10 (c)) shows that the switching is occurring over a relatively wide frequency range. Adding the zero sequence current to the measured currents the switching becomes more uniform, as can be observed in the phase current and gate signals (Fig. 10 (d)), or directly by the instantaneous switching frequency (Fig. 10 (e)) and the current spectrum (Fig. 10 (f)) that becomes more uniform. Modulating the hysteresis band (Fig. 10 (g)) the switching frequency becomes almost constant (Fig. 10 (h)) and the spectrum is more centered around 4kHz (Fig. 10 (i)).

The decoupling does not affect the fast dynamic response inherent in the hysteresis controller as can be seen in the power reference step change (Fig. 11). Fig. 11(a) shows the estimated active power (p) quickly tracking the active power reference (p_{ref}) during a step from 40% to 80%. A rise time of 500μs is observed in the positive step (Fig. 11(b)). The active power step does not have any influence on the reactive power (q) as shown in Fig. 11(b).

V. VF-DHC WITH LCL FILTER

The VF-DHC concept can be extended for high power applications where it is very difficult to meet the IEEE519 without a third order filter. The LCL filter attenuates the switching ripple substantially and the overall size of the LCL filter is reduced compared to only an L filter. However, systems incorporating LCL filter requires extra control effort in order to compensate some undesirable characteristics such as the filter resonance. The modified VF-DHC showed in Fig. 12 maintains the core of the conventional approach and incorporates outer control loops which damp the filter resonance, reject the influence of grid voltage

harmonics and compensate for the reactive power of the capacitor filter, since the active and reactive power are controlled on the inverter side.

Another issue that has to be considered is the grid virtual-flux estimation, which differs from the concept with a series inductor as a filter. In this case the grid side inductor (L_g) flux has to be considered and results in

$$\bar{\psi}_g = \int \bar{u}_{inv} \cdot dt - L_{inv} \cdot \bar{i}_{inv} - L_g \cdot \left(\bar{i}_{inv} - \bar{i}_c\right) \tag{18}$$

An active damping strategy can be applied effectively because the resonance frequency of the output filter is usually inside the bandwidth of the inverter control loops. The active damping is achieved by emulating a resistor in parallel with the filter capacitor by creating a current source proportional to the capacitor voltage resonance component

Since the damping strategy is based on the capacitor voltage, any harmonic presented in the grid will be amplified through the damping feedback. Therefore, a harmonic control method has to be implemented in order to reduce the effect of such harmonics.

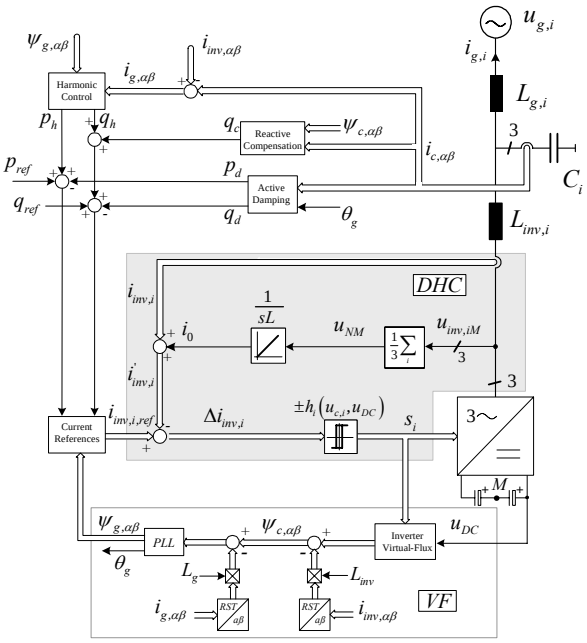

Fig. 12 - Extension of the VF-DHC for high power application where LCL filter is usually employed.

The harmonic control block proposed in [9][10] regulates the harmonics individually in their respective individual synchronous reference frame. Each harmonic quantity to be controlled is transformed into its own individual synchronous reference frame. The corresponding harmonic quantities appear as dc in their own reference frame, consequently a PI control is enough to guarantee zero steady state error.

Bothe active damping and harmonic control components are transformed to power quantities and add to the active and reactive power references as shown in Fig. 12.

The estimated capacitor reactive power (19) is added to the reactive power reference (Fig. 12) in order to compensate the effect of the output filter capacitor

$$q_c = \frac{3}{2}\omega \cdot (\psi_{c,\alpha} \cdot i_{c,\alpha} + \psi_{c,\beta} \cdot i_{c,\beta}) \tag{19}$$

VI. EXPERIMENTAL VERIFICATION

The experimental verification of active damping, harmonic control and reactive power compensation schemes is performed using the 6kW inverter setup described for the L filter VF-DHC approach, except the output filter that was replaced by a third order LCL filter (L_{inv}=7.9mH, L_g=3.5mH and C=14.1μF). The sample rate of the main loop was reduced to 140kHz due to the limited computation time, since further calculations are required in the outer loops. The active damping calculation was included in the 30kHz loop. Additionally, in order to calculate the 5th harmonic control a slower loop with sample rate of 10kHz is included in the DSP code.

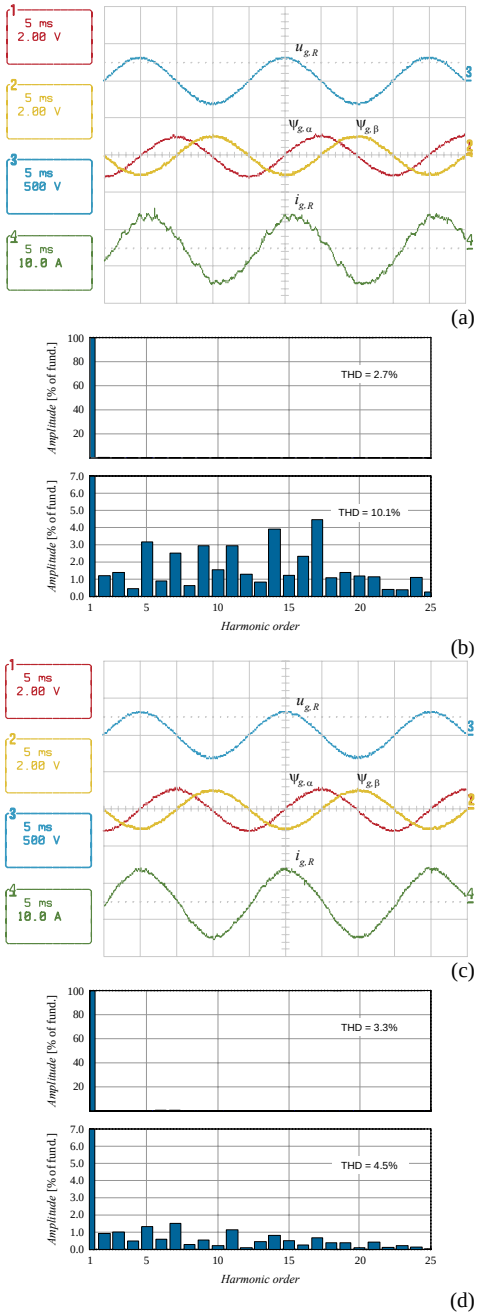

Fig. 13 – Experimental result of grid phase voltage $u_{g,R}$, virtual-flux $\psi_{g,\alpha\beta}$ and phase current $i_{g,R}$ (a) for the conventional VF-DHC and (c) the extended strategy including the active damping, harmonic control and reactive power compensation. The respective grid voltage and current harmonic spectrums are shown in (b) and (d).

The effectiveness of the extended approach concerning the LCL resonance damping, the 5th harmonic reduction and the capacitor reactive power compensation is observed comparing phase current ($i_{g,R}$) and current spectrum of the conventional VF-DHC (Fig. 13(a)-(b)) with the proposed VF-DHC (Fig. 13(c)-(d)). The resonance component presented in the current spectrum of the conventional scheme (Fig. 13(b)) is well damped in the extended method (Fig. 13(d)). The same behaviour is observed in the 5th harmonic component that is reduced from 3% to around 1.3%.

A correction in the reactive power is also observed when comparing the phase shift between grid voltage, $u_{g,R}$, and current, $i_{g,R}$, for the conventional approach (Fig. 13(a)) and the extend method (Fig. 13(c)).

Fig. 14 shows the experimental results of dynamic response when a step from 40% to 80% of total active power is given. A significant reduction of the resonance oscillation is noted comparing the VF-DHC (Fig. 14 (a)) and the extended method (Fig. 14 (b)). It can be noted that even including the outer loops fast tracking (1ms) of the active power reference (p_{ref}) is maintained.

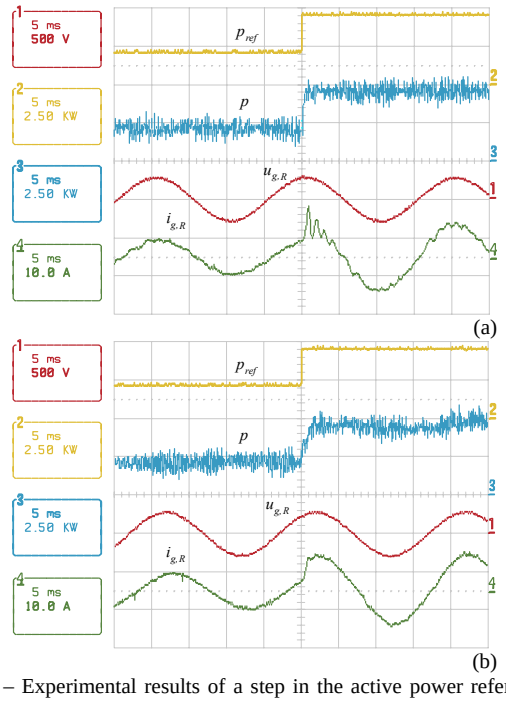

Fig. 14 – Experimental results of a step in the active power reference of 40% with (a) the conventional VF-DHC and (b) the extended system. Active power reference p_{ref}, actual active and reactive power p and q respectively, grid phase voltage $u_{g,R}$ and current $i_{g,R}$.

VII. CONCLUSIONS

This paper has proposed a control concept for mains connected inverters applications that combines a decoupling hysteresis current control with virtual-flux and power estimation methods so that the advantages of a fast dynamic response and relatively simple implementation are maintained. The interference between phases for three-phase, three-wire inverters using conventional hysteresis control is avoided when decoupling hysteresis control is used. By using a varying hysteresis band the switching frequency can be made almost constant. Both control strategies, Virtal-Flux Current Hysteresis Control (VF-CHC) and Virtual-Flux Decoupling Hysteresis Control (VF-DHC) have been verified through simulation and experimental implementation.

Active damping and harmonic control have been incorporated in the proposed concept in order to extend the method for high power applications, where usually a third order filter is used as output filter. The performance of the extended method was also experimentally verified.

VIII. REFERENCES

[1] J. Holtz, “Pulsewidth Modulation - A survey,” IEEE Transactions on Industry Electronics, Vol. 39, No. 5, Oct. 1992, pp. 410-420.

[2] T. Noguchi, H. Tomiki, S. Kondo and I. Takahashi, “Direct Power Control of PWM Converter without Power-Source Voltage Sensors,” IEEE Transactions on Industry Applications, Vol. 34, No. 3, May/June 1998, pp. 473-479.

[3] M. Malinowski, M. J. Jasinski and M.P. Kazmierkowski, “Simple Direct Power Control of Three-Phase PWM Rectifier Using Space-Vector Modulation (DPC-SVM),” IEEE Transactions on Industry Applications, Vol. 51, No. 2, April 2004, pp. 447-454.

[4] L. Malesani and P. Tenti, “A Novel Hysteresis Control Method for Current-Controlled Voltage-Source PWM Inverter with Constant Modulation Frequency,” IEEE Transactions on Industry Applications, Vol. 26, No. 1, Jan/Fev 1990, pp. 88-92.

[5] Q. Yao and D.G. Holmes, “A Simple, Novel Method for Variable-Hysteresis-Band Current Control of a Three Phase Inverter with Constant Switching Frequency,” in Proc. IAS’93, Vol.2, Oct. 1993, pp. 1122-1129.

[6] L. Dalessandro, U. Drofenik, S.D. Round and J.W. Kolar, “A Novel Hysteresis Current Control for Three-Phase Three Level Rectifiers,” in Proc. APEC’05, Vol.2, Mar. 2005, pp. 501-507.

[7] S. D. Round, L. Dalessandro and J. W. Kolar, “Novel Phase Decoupling and Coordinating Tolerance Band Current Control for Three-Phase Three-Level PWM Rectifiers,” in Proc. PCIM’05, Jun. 2005, pp. 285-291.

[8] Malinowski, M. P. Kazmierkowski, S. Hansen, F. Blaabjerg and G. D. Marques, “Virtual-Flux-Based Direct Power Control of Three-Phase PWM Rectifiers,” IEEE Transactions on Industry Applications, Vol. 37, No. 4, July/Aug. 2001, pp. 1019-1027.

[9] L. A. Serpa, S. Ponnaluri, P. M. Barbosa and J.W. Kolar, “A Modified Direct Power Control Strategy Allowing the Connection of Three-Phase Inverter to the Grid through LCL Filters,” in Proc. IAS’05, Vol. 1, Oct. 2005, pp. 565-571.

[10] S. Ponnaluri and A. Brickwedde, “Overriding Individual Harmonic Current Control with fast dynamics for Active Filtering,” Proc. PESC’01, June 2001, pp. 1596-1601.